# Depth imaging with crooked 2D and irregular 3D seismic data in rugged terrain

*Daniel R.H. O'Connell*, Fugro Consultants, Kyle Brock, Goran Stankovic, and Nebojsa Pralica, Agile Seismic, and Dengguo Zhou and Weizhong Wang, GeoTomo*

**Summary**

Due to permit restrictions, crooked 2D and irregular 3D seismic reflection data were acquired within a 330 km$^2$ area in central coastal California to image geologic structure and faults from the near-surface to depth of > 10 km. Key steps to achieve successful depth imaging included, non-stationary coherent noise modeling and removal, 3D processing of all 2D and 3D data, 3D tomography, residual statics using first-arrivals, and adaptive fast beam migration. No sonic log velocity data were available so multiple stages of 3D velocity inversion including joint velocity-density inversion with gravity data were used to develop velocity models and statics for prestack-depth-migration velocity analyses. Improved signal-to-noise in the 3D volumes provided constraints to design wavenumber spectral-balancing and wavelet transform denoising parameters to improve imaging in the 2D data.

**Introduction**

Seismic reflection data were acquired over two years within an area of about 330 km$^2$ in the central California coast to characterize the geometry and sense of slip of active faults near the Diablo Canyon Power Plant. Permitting restrictions limited seismic sources most receivers to roads resulting in extremely crooked 2D and irregular 3D seismic reflection data (Figure 1). No sonic log velocity constraints were available from within the imaging volume so 3D tomography was used to develop velocity models and statics. The geologic structure is complex with shallow and lateral acoustic velocities varying between 400 m/s and 6000 m/s. The highly variable velocities and rugged terrain produced texture that more substantially exceeds the texture resulting from the reflecting layers than is common in typical land seismic data (Claerbout and Black, 2005). Ground vibrations and noise from mechanical, hydraulic, and electrical transmission lines resulted in ground vibration noise on the order of 1% g near the power plant. Consequently, several strategies were developed to cancel coherent noise in the data acquisition and processing to provide sufficient signal-to-noise to pick first arrivals and accomplish tomographic and depth imaging objectives.

**Data**

3D data were acquired using 64,000 lb and 17,000 lb Vibroseis sources. A 450 lb AWD was used for high-resolution 2D data acquisition. Receivers acquired data at group spacings ranging from 5 m to 91 m with a mixture of single-channel nodes, multi-channel nodes with receiver group arrays, and a 2D cable system with receiver group arrays. Permitting restrictions required the use of single-channel-single-geophone nodes over large areas. Topographic relief was about 600 m overall with deeply incised valleys that produced local topographic relief on the order of 100-200 m.

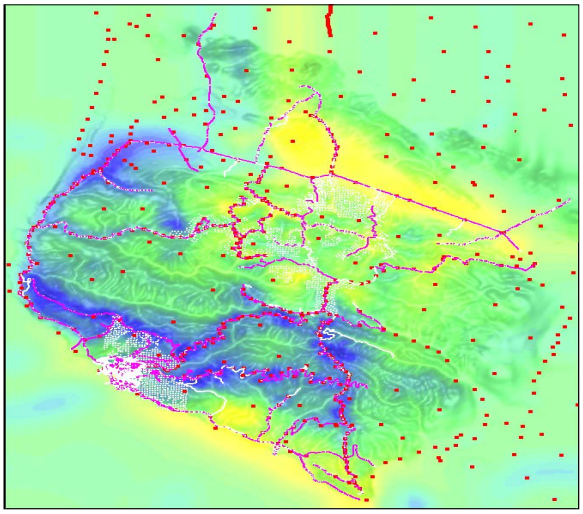

Figure 1: Geometry of seismic acquisition (source in magenta and receiver in white) and gravity observation (red dots).

**Coherent Noise Reduction Approach**

During the second year of data acquisition near the power plant a geophone array was installed near the turbines that were the source of large coherent 30 Hz ground vibration to provide 30 Hz vibration phase triggering capabilities. An even number of sweeps were used with the individual pairs of sweeps started at 180 degrees apart relative to the phase of the 30 Hz ground vibrations. This reduced 30 Hz coherent noise by 12-24 db and provided sufficient dynamic range in the recording systems to model and subtract remaining coherent noise during processing.

Figure 2a shows typical data from near the power plant with strong 30 Hz mechanical vibration and 60 Hz electrical noise that obscures the first breaks and reflections. We designed a noise-cancelation approach that uses the



DOI http://dx.doi.org/10.1190/segam2014-1651.1

total power of the receiver time windows and finds the amplitude and initial phase of coherent sinusoidal signals, that when subtracted from the data minimize the total power of the data. This approach allows attenuation of coherent noise while preserving signal. The data from a single receiver channel as a function of time be $v(t)$ and the coherent noise model for a single frequency, $f$, be $n(t,f)$. The noise model as a single frequency is:

$$n(t,f) = A(f) * \sin\left(2\pi f t + \varphi(f)\right) \qquad (1)$$

where $A(f)$ is the scalar noise amplitude and $\varphi(f)$ is the scalar initial phase. At each frequency, $f_j$, we minimize the total power, $P$, over all the samples in the channel's shot window, $i=1,m_t$, given by:

$$P = \sum_{i=1}^{m_t} \left( (v(t_i) - \sum_{j=1}^{m_f} n(t_i, f_j)) \right)^2 \qquad (2)$$

This process is done by stepping through $j=1,m_f$, to incrementally solve for the A(fj) and $\varphi(f_j)$ at each frequency, $f_j$, then moving on to the next frequency. At each frequency trial values of $\varphi(f_j)$ of 0, π, 2*π, and 3*π are used to find the initial minimum of (2) with an initial value of $A(f_j)$ =0.1*max(abs($v(t)$). Then Powell's method (Press et al., 2007) is used to search and find values of $A(f_j)$ and $\varphi(f_j)$ that minimize (2).

This approach can be applied prior to ensemble stack to effectively phase lock on the coherent 30 Hz vibrations and 60 Hz electrical noise. When applied after ensemble stack, it was necessary to search for at least two additional frequencies slightly less than and greater than 30 Hz and 60 Hz to account for the slightly phase and frequency shifts introduced by ensemble-stacking the coherent noise that can be slightly out of phase between the individual ensemble records. A frequency step of 0.025 Hz was used to grid search between 59 and 60 Hz and 60 Hz and 61 Hz for two additional frequencies to apply further coherent noise attenuation. If no reduction in (2) was found, no additional coherent noise was subtracted from the data. This approach was tested using vertically-stacked data. The strategy to search for two additional coherent frequencies slightly less than and greater than 60 Hz effectively canceled the broad coherent noise peak centered at 60 Hz in Figure 2 without removing signal.

The effectiveness of the noise-attenuation approach is demonstrated with a shot-gather shown near the power plant that was bandpass-filtered from 25 Hz to 84 Hz, scaled by time to show the first-breaks and higher-frequency reflections, and normalized by the maximum absolute amplitude of each trace; strong coherent 30 Hz and 60 Hz noise dominates the shot gather even when notch filters are applied at 30 Hz and 60 Hz (Figure 3a).

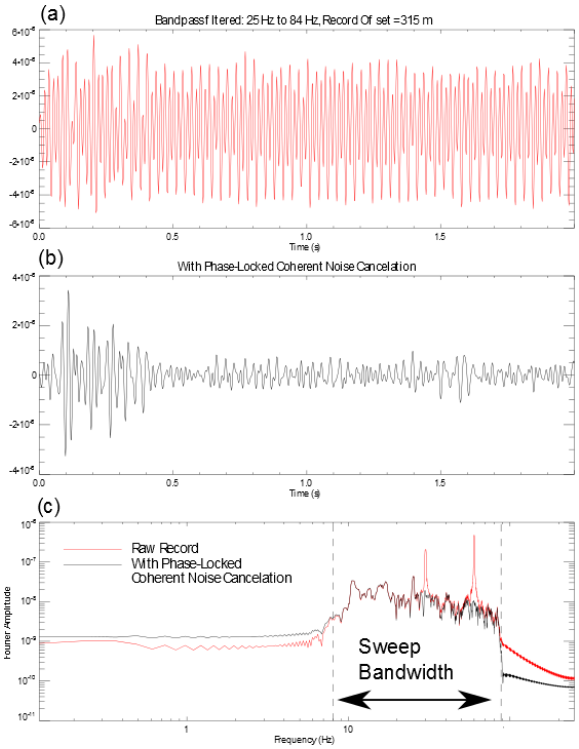


Figure 2: Bandpass-filtered trace (a), phase-locked noise attenuation result (b), and Fourier amplitude (c) of (a) and (b).

While the first-arrival is apparent through most of the band-reject and bandpass-filtered shot-gather in Figure 3a it is often difficult to discern the first-arrival on individual channels. In contrast, after coherent-noise attenuation, the first-breaks are consistently apparent in the shot gather as well as reflections and diffractions from the subsurface (Figure 3b). The "jitter" in the first-break arrival times is associated with the large thickness variations of ~500 m/s shallow soil. Some of the receivers in Figure 3 are located on thick soil and others on thin soil. The difference in soil thickness produces about a 30 ms first-break arrival time variability that is essentially a receiver static.

**Depth Imaging Processing Approach**

The essential elements of the processing approach are listed in Figure 4. Initial processing approaches, including 5D interpolation to compensate for the irregular acquisition geometry where not successful; velocity ambiguities persisted in the prestack-depth migration velocity analyses. Initial traveltime tomography and joint traveltime-gravity



DOI http://dx.doi.org/10.1190/segam2014-1651.1

inversions improved velocity constraints but velocity resolution was not sufficient over a large enough area to eliminate velocity ambiguities in the selection of velocities during prestack depth-migration velocity analyses. Consequently, more gravity data were collected over a wider area (Figure 1) to provide additional constraints for joint traveltime-gravity inversion (Langenheim, 2014). These additional gravity data and the application of joint traveltime-gravity inversion were the key initial steps in processing sequence that eliminated ambiguities in the prestack depth-migration velocity analyses.

The complex shallow velocity structure, rugged topography, and variable signal-to-noise presented challenges for surface-consistent statics estimation. The 3D traveltime tomography provided the information needed to apply the method of Hatherly et al. (1994) to use the first arrival wavefield to constrain surface-consistent residual statics. The 3D tomography synthetic travel times and long-wavelength statics solution were used to align the first-arrival wavefields within time windows that were input into surface-consistent residual statics calculations. This step proved crucial to achieve sufficient consistent signal-to-noise to perform the iterative prestack depth-migration velocity analyses.

Testing of Kirchhoff and fast beam migration (FBM) with the synthetic Canadian Foothills model (Gray and Marfurt, 1995) showed that FBM provided the best imaging of faults, particular as depth increased. Other migration approaches like reverse-time migration (RTM) were not feasible given the highly irregular acquisition geometry and inability of 5D interpolation to effectively regularize the data geometry. Migrations of all the larger-scale data were done using FBM since it accounts for the multipathing that was prevalent throughout the project area due to substantial 3D velocity variability. FBM was applied in 3D to all data; 2D line data simply consisted of linear to sinuous source-receiver paths but were migrated to CDP positions in 3D.

The higher signal quality was found in 3D volumes in areas of more regular acquisition geometry and provided constraints to evaluate post-processing approaches to improve signal-to-noise in the 2D data. Scattered surface waves, vehicle traffic, and mechanical equipment produced sometimes strong lower frequency noise, particularly along acquisition routes through narrow valleys floored by thin soft sediment. Time-variant filtering, AGC, and wavenumber spectral balancing provided effective improvements in 2D signal-to-noise in many cases, but additional wavelet transform denoising was often required in certain areas to produce 2D images consistent with 3D data in areas where 2D data intersected 3D volumes.

Wavelet transforms of the 2D depth data were done using the Symlet wavelet function that is similar to the zero-phase Vibroseis wavelet. The wavelet transform is calculated and then a stack constructed of wavelet reconstructions that discard wavelet coefficients with the lowest power below a total power threshold. By stepping through wavelet reconstructions at total retained power between 66-90% and 100% at 1% increments and stacking each reconstruction noise in the 2D images was effectively reduced to produce fidelity of the 2D imaging with intersected 3D volumes.

**Conclusions**

In a region with complex 3D velocity variations where sonic log velocity constraints are sparse or nonexistent, 3D tomography using traveltime and gravity data can provide sufficient constraints to develop a successful depth imaging processing flow. Initial application of this approach from irregular 3D and crooked 2D data from the central California coast using existing gravity data failed to obtain sufficient constraints to unambiguously update velocities using prestack depth-migration velocity analyses. Acquisition of new gravity data within the project area provide sufficient additional constraints when used in a joint traveltime-gravity inversion to obtain the final starting point to calculate final surface-consistent residual statics and successfully iterate through the prestack depth-migration velocity analyses. The highly adaptive FBM approach to migration provided the ability to obtain migration quality comparable to RTM using data constrained to highly irregular acquisition geometry in an area with extreme 3D velocity variability.



DOI http://dx.doi.org/10.1190/segam2014-1651.1

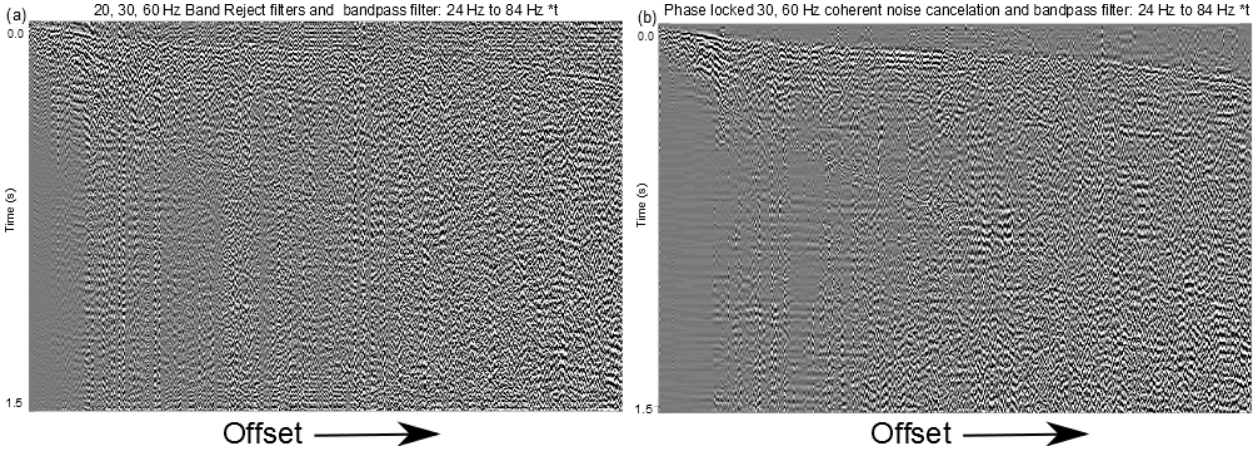


Figure 3: Shot gather with bandpass filter from 24 Hz to 84 Hz from within the power plant area. Bandrejection filters at 20 Hz, 30Hz, and 60 Hz are also applied in (a). Phase-locked coherent noise cancellation is used in (b). Traces are ordered by offset from left (~10 m) to right (~600 m).

## Sonic-Log-Free Processing Approach

- **3D processing of all data ("2D" crooked profiles and irregular 3D)**
- **Joint travel-time-gravity 3D tomography for initial 3D interval velocity model and long-wavelength statics**
- **3D tomography refraction moveout first-break residual statics**
- 3D surface-consistent processing (amplitude, decon, statics, etc.)
- 3D Fast Beam Pre-stack Depth Migration (FBM) velocity updates
- 3D FBM/Kirchhoff PSDM
- 3D migration stacks
- 2D post-processing including time-variant filtering, AGC, wavelet-transform denoise
- 3D post processing
- 3D attributes

Figure 4: Key depth- imaging processing steps.





DOI http://dx.doi.org/10.1190/segam2014-1651.1

http://dx.doi.org/10.1190/segam2014-1651.1

**EDITED REFERENCES**

Note: This reference list is a copy-edited version of the reference list submitted by the author. Reference lists for the 2014 SEG Technical Program Expanded Abstracts have been copy edited so that references provided with the online metadata for each paper will achieve a high degree of linking to cited sources that appear on the Web.

**REFERENCES**

Claerbout, J. F., and J. L. Black, 2005, Basic earth imaging (version 2.4): Classroom text, accessed 26 June 2014, sepwww.stanford.edu/sep/prof/bei1005.pdf.

Gray, S. H., and K. J. Marfurt, 1995, Migration from topography: Improving the near-surface image: Canadian Journal of Exploration Geophysics, **31**, no. 1-2, 18–24.

Hatherly, P. J., M. Urosevic, A. Lambourne, and B. J. Evans, 1994, A simple approach to calculating refraction statics corrections: Geophysics, **59**, 156–160, http://dx.doi.org/10.1190/1.1443527.

Langenheim, V. E., 2014, Gravity, aeromagnetic and rock-property data of the central California coast ranges: U. S. Geological Survey Open-File Report 2013-1282.